Existence and stability of accelerating solitons in sliding-frequency filter systems

M. Facão*
Departamento de Física, Universidade de Aveiro, Campus Universitário de Santiago, 3810-193 Aveiro, Portugal

D. F. Parker†
School of Mathematics and Statistics, University of Edinburgh, The King's Buildings, Edinburgh EH9 3JZ, United Kingdom
(Received 27 January 2005; published 28 June 2005)

Sliding-frequency filter systems are known to admit two families of accelerating solitons: high-amplitude and low-amplitude families. Such equilibrium solutions are computed here, for a wide range of filter strengths, as self-similar solutions having Airy function asymptotics. In a limited parameter region, the profile possesses a secondary small hump. The high-amplitude solitons are found to be stable over a region of parameter space which is here determined by the Evans function method, adjusted to Airy function asymptotics. The loss of stability is due to a Hopf bifurcation.

DOI: 10.1103/PhysRevE.71.066611 PACS number(s): 42.65.Tg, 42.65.Sf, 42.81.Dp

I. INTRODUCTION

Sliding-frequency filtering refers to a technique used to control the noise growth in soliton-based optical communication systems. Real soliton-based systems require repeated amplification to overcome material attenuation. The amplification, in turn, introduces noise produced by spontaneous emission. This noise may be suppressed by the use of one filter in each amplification stage. The filtering is known to be more effective if the peak frequency is slightly shifted from one filter to the next, using a technique known as sliding-frequency filtering.

The propagation of pulses over large distances in such systems is governed by the following equation [1]:

$$iq_Z + \tfrac{1}{2}q_{TT} + |q|^2 q = i\delta q + i\beta\{\partial_T + i\sigma Z\}^2 q, \qquad (1)$$

where q is the normalized complex envelope of the pulse, Z and T are the normalized distance along the fiber and retarded time, respectively, δ and β are normalized and averaged (over the amplifier distance) parameters for excess gain and filter strength, and σ is the normalized sliding rate. Equation (1) admits steady profile solutions that evolve along an accelerating time path, i.e., accelerating solutions. This has been known since the time the technique was suggested. Parameter regions of the existence and stability of such solutions have been defined by numerical and experimental results [2] and mainly compared with results from perturbation approaches [3–5]. Such approaches were first investigated by perturbing around the sech soliton solution of the nonlinear Schrödinger equation [3,4], but, more recently, the zero-order ansatz was more general than the sech soliton [5]. The general results obtained previously may be summarized as follows. For fixed filter strength and sliding rate, there is a lower gain threshold below which pulses do not exist. Above this threshold, there are two families of solutions differing in peak amplitude (or energy) and in velocity. The low-amplitude family is unstable and the high-amplitude family is stable up to an upper limit of gain which meets the lower gain threshold for values of filter strength around 0.85 [2,4].

In agreement with the existence of accelerating solutions, Eq. (1) was recently reduced to an ordinary differential equation (ODE) using an accelerating similarity variable [6]. Here we show that the asymptotics of the resulting ODE is associated with Airy functions, a fact that is then used in Sec. II to search for localized solutions. In Sec. III, we obtain the stability eigenvalue problem whose asymptotics are also associated with Airy functions. The similarity of this stability eigenvalue problem with the one arising for self-bending photorefractive solitons permits us to apply an Evans function methodology similar to that in [7]. Hence, in Sec. IV, we define a modified Evans function and apply the method to find the stability eigenmodes focusing especially on those that are responsible for the loss of stability exhibited by the high-amplitude family of solutions. In Sec. V, direct numerical integration of Eq. (1) is used to confirm the stability results obtained in the previous section.

II. EQUILIBRIUM SOLUTIONS

The accelerating solutions of Eq. (1) were recently related to the accelerating similarity variable given by $\zeta = T + (\sigma/2)Z^2 + bZ + \zeta_0$ (with b and ζ_0 arbitrary constants) [6]. Introducing the ansatz $q(Z,T) = e^{i\theta(Z,\zeta)}W(\zeta)$ (with θ real and W complex) into Eq. (1) yields

$$\theta(Z,\zeta) = -\sigma\zeta Z + b\sigma\frac{Z^2}{2} + \sigma^2\frac{Z^3}{6} + c_1 \qquad (2)$$

and

$$(1+4\beta^2)W'' + 2(1+2i\beta)ibW' + 2(1+2i\beta)(\sigma\zeta - i\delta + |W|^2)W = 0, \qquad (3)$$

where c_1 is an arbitrary constant. Applying the change of variables

$$W(\zeta) = [\sigma^2(1+4\beta^2)]^{1/6} w(y),$$

*Electronic address: mfacao@fis.ua.pt
†Electronic address: D.F.Parker@ed.ac.uk

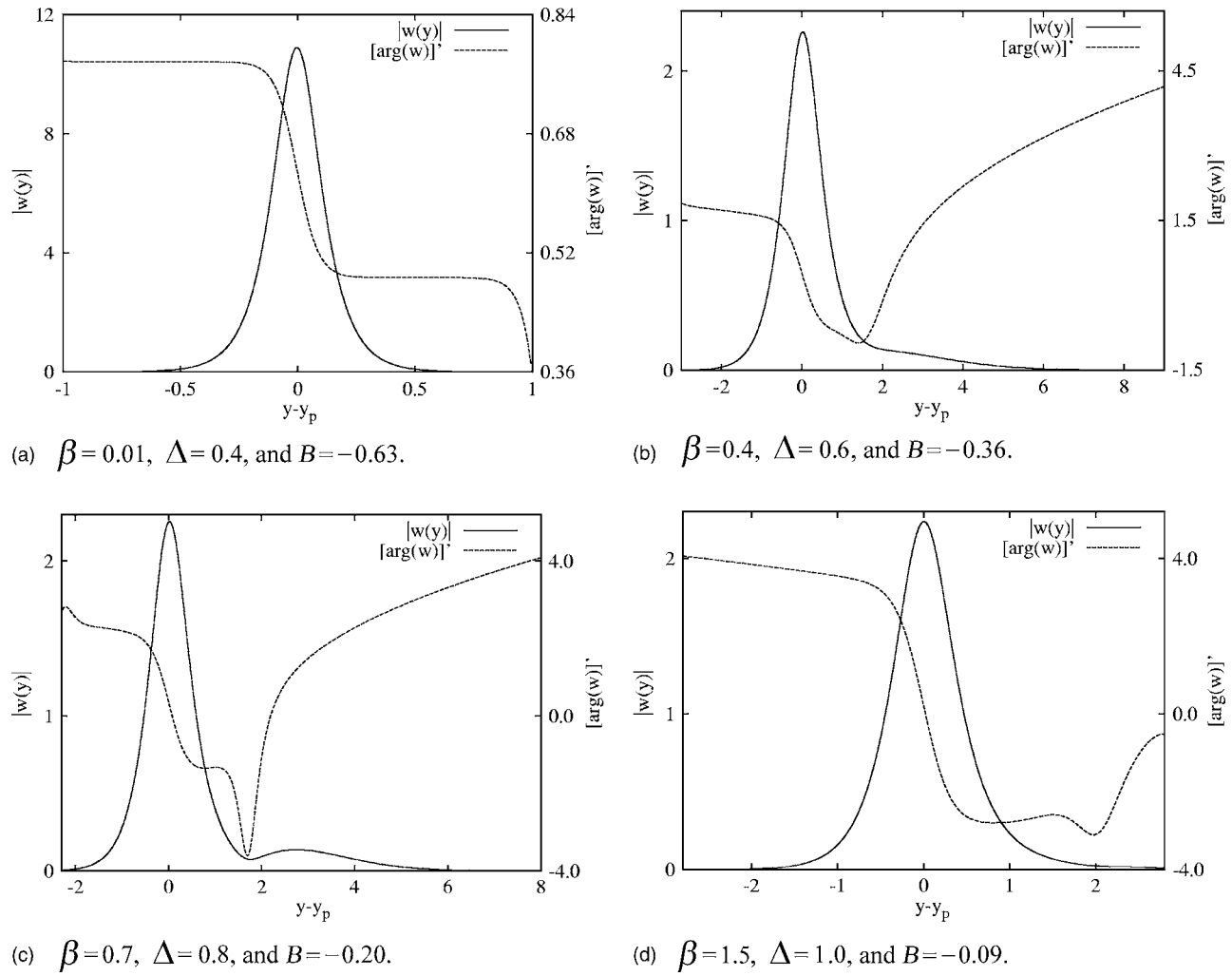

FIG. 1. Pulse profile and chirp for B_s solutions.

$$\sigma\zeta = [\sigma^2(1+4\beta^2)]^{1/3} y,$$

transforms the ordinary differential Eq. (3) to

$$w'' + 2(1+2i\beta)\{iBw' + (y - i\Delta + |w|^2)w\} = 0, \tag{4}$$

where $B=[\sigma^{1/2}(1+4\beta^2)]^{-2/3}b$ and $\Delta=[\sigma^2(1+4\beta^2)]^{-1/3}\delta$. Perturbation around the function $w(y)=\Gamma\,\mathrm{sech}[\Gamma(y-y_p)]\mathrm{e}^{-iBy}$ (where $\Gamma^2=-B^2-2y_p$ and y_p is the peak position) show that the permitted velocities B for a single-peak pulse should be approximately equal to the negative roots of the following cubic equation [3,6]:

$$4\beta B^3 - 4\Delta B - 1 = 0. \tag{5}$$

Negative roots exist only for $\Delta \geqslant \frac{3}{4}\beta^{1/3}$; one when the equality is satisfied and two in the general case.

For Eq. (4), pulselike solutions must have $w(y)$ and $w'(y)$ tending to zero as $|y| \to \infty$. Thus away from the pulse, Eq. (4) may be approximated as

$$w'' + 2(1+2i\beta)\{iBw' + (y - i\Delta)w\} = 0, \tag{6}$$

to which we may apply the transformation given by

$$w(y) = \mathcal{W}(z)\exp[-iB(1+2i\beta)y] \tag{7}$$

and

$$z(y) = (2+4i\beta)^{1/3}\left\{-y + i\Delta - (1+2i\beta)\frac{B^2}{2}\right\}, \tag{8}$$

thus yielding the Airy equation defined in the complex z plane, namely

$$\mathcal{W}'' - z\mathcal{W} = 0.$$

This result shows that solutions to the ODE (4) have Airy function asymptotics. Under transformation (8), the real domain for y is mapped into a line in the complex z plane, inclined at angle $\phi=\frac{1}{3}\arg(2+4i\beta)$ [the principal branch of the cube root appearing in expression (8) is chosen] and crossing the real axis at $(4+16\beta^2)^{1/6}(\Delta-\beta B^2)/\sin\phi$. The Airy functions that asymptotically tend to zero as $|z| \to \infty$ depend on $\arg(z)$. Standard theory of Airy functions defines three functions $\mathrm{Ai}_0(z)$, $\mathrm{Ai}_1(z)=\mathrm{Ai}(z\mathrm{e}^{-2\pi i/3})$, and $\mathrm{Ai}_{-1}(z)=\mathrm{Ai}(z\mathrm{e}^{2\pi i/3})$, and three $2\pi/3$ sectors S_0, S_1, and S_{-1} [8]. For $z \in S_j$, only $\mathrm{Ai}_j(z)$ is exponentially decaying as $|z| \to \infty$; $\mathrm{Ai}_j(z)$ is known as the *recessive* solution in S_j. For pulselike solu-

tions to Eq. (4), the large positive and negative values of y correspond to z values within the sectors S_{-1} and S_0, so that the appropriate recessive Airy solutions are $\mathrm{Ai}_{-1}[z(y)]$ as $y\to+\infty$ and $\mathrm{Ai}_0[z(y)]$ as $y\to-\infty$. Note that $w(y)$ is obtained from $\mathcal{W}(z)$ through Eq. (7), whose exponential modulus is $\exp(2\beta By)$ (with $B<0$ and $\beta>0$). Assuming that $\mathcal{W}(z)$ has the exponential decay of $\mathrm{Ai}_0[z(y)]$ as $y\to-\infty$, $w(y)$ also decays exponentially, since the rate of exponential decay of $\mathrm{Ai}_0[z(y)]$ for large $z\in S_0$ is proportional to $y^{3/2}$, which dominates the linear rate of exponential growth introduced through transformation (7).

The numerical search for localized solutions to Eq. (4) used the following shooting procedure. For fixed β and Δ, we find the two negative roots of Eq. (5), which we name $\bar{B}_s$ and $\bar{B}_l$ (s and l stand for small and large absolute values, respectively). They constitute the starting estimates $\bar{B}$ for B. For each one, we follow Parker *et al.* [6] to estimate a location $\bar{y}_1$ on the left tail ($\bar{y}_1<y_p$) where $w\sim\epsilon$. Near $\bar{y}_1$, the solution $w(y)$ should be well described by $\mathrm{Ai}_0[z(y)]$ through Eq. (7). Thus at $y=\bar{y}_1$, the initial conditions are

$$w(\bar{y}_1)=c_1\mathrm{Ai}_0[z(\bar{y}_1)]\exp[-i\bar{B}(1+2i\beta)\bar{y}_1]=\epsilon,$$

$$w'(\bar{y}_1)=-c_1\exp[-i\bar{B}(1+2i\beta)\bar{y}_1]\times\{(2+4i\beta)^{1/3}\mathrm{Ai}_0'[z(\bar{y}_1)]+i\bar{B}(1+2i\beta)\mathrm{Ai}_0[z(\bar{y}_1)]\}.$$

We start a forward integration from $\bar{y}_1$ and, after passing through a maximum of $|w|$, we stop when a minimum of $|w|^2+|w'|^2$ is reached. Then y_1 and B are adjusted in order to minimize $|w|^2+|w'|^2$ down to ϵ^2 or smaller. A similar shooting procedure could start at a location on the right tail, say $y=\bar{y}_2$. In this case, the initial conditions should use the appropriate recessive Airy function at $z(\bar{y}_2)$ which is $\mathrm{Ai}_{-1}(z)$.

We have searched for pulse profiles containing a single pulse throughout the region of the parameter space (β,Δ) covering β from 0.005 to 2.0 and Δ from $\frac{3}{4}\beta^{1/3}$ to 3.5. The lower boundary, $\Delta\geqslant\frac{3}{4}\beta^{1/3}$, arises from the estimates of B using the cubic Eq. (5), based on sech profiles.

Results concerning B_s are described first. For values of β up to 0.35, localized solutions are found right from the boundary $\Delta=\frac{3}{4}\beta^{1/3}$. However, for $\beta>0.35$, existence requires substantially larger Δ (see Fig. 4). This deviation from the existence curve predicted by perturbation theory was already found from approximately the same β value, by numerical simulation of Eq. (1) using initial sech pulses [2]. The upper boundary for existence is of little importance, since the stability/instability threshold (see Sec. IV) is reached for smaller Δ values. Hence, for $\beta<0.5$, pulses have been constructed just in $\Delta\leqslant3.5$. For larger β, the curve of existence experiences a quick drop down to $\Delta\simeq2.0$ where it remains while β increases up to ~2.0. For fixed β, the absolute value of the velocity B decreases as Δ increases and the profile peak amplitude increases with Δ. For small β, the pulse profiles are very close to sech profiles, and the phase has chirp which is close to a tanh behavior [Fig. 1(a)]. However, as β increases, the deviations from this behavior become more noticeable. The pulse profiles become asymmetric and thinner than the approximating sech pulse of [3]. This asymmetry is more evident for small values of Δ with (β,Δ) close to the existence boundary but, for $\beta\leqslant0.88$, it is present for values of Δ up to the stability boundary. Whenever the shooting method described above starts at the left-hand side, it produces these asymmetrical pulses with a pronounced right tail. However, whenever these pulses are used as initial conditions for the full numerical integration of Eq. (1), the output profiles are found to be more asymmetric or even to have a secondary hump on the right. The disagreement between the obtained self-similar solution and the actual equilibrium pulse is due to the shooting strategy which minimizes $|w|^2+|w'|^2$ instead of searching for a right tail behavior coincident with the behavior of $\mathrm{Ai}_{-1}(z)$. The shooting method was then improved in order to compute such equilibrium solutions. The procedure involved a first estimation of B and y_2 by the method described above and a second estimation of y_2 using backward integration which uses $\mathrm{Ai}_{-1}[z(y_2)]$ and allows the existence of two humps. Finally, a further optimization of B and y_2 is achieved using backward integration and minimization of $|w|^2+|w'|^2$ at the left tail. Figures 1(b) and 1(c) show profiles and chirps of two solutions obtained by this improved shooting technique. Figure 1(d) shows one self-similar solution for β and Δ outside the region of stability. The profile is more symmetric than the

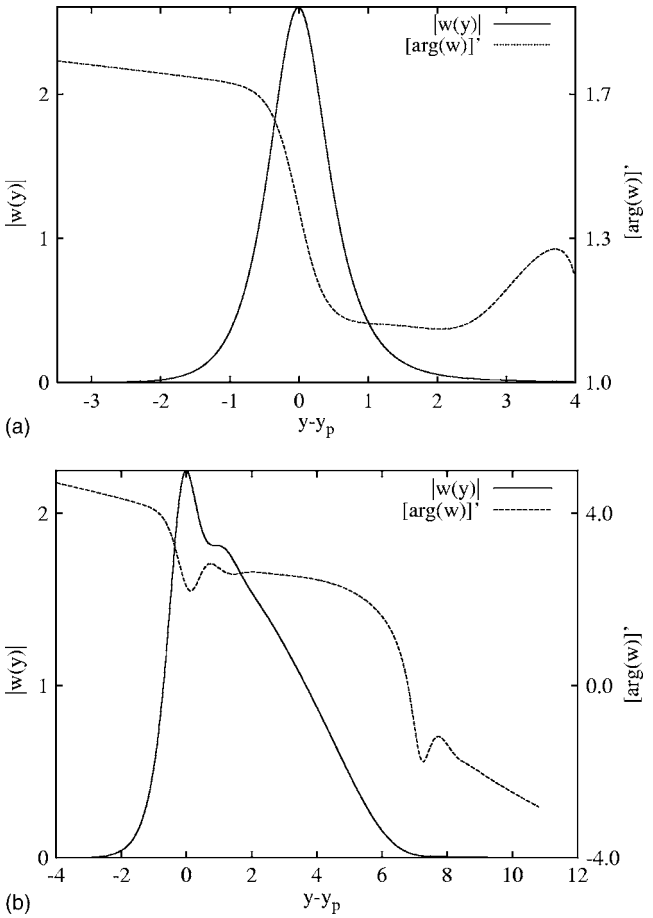

FIG. 2. Pulse profile and chirp for two B_l solutions: (a) $\beta=0.08$, $\Delta=0.33$, and $B=-1.40$ and (b) $\beta=1.0$, $\Delta=1.5$, and $B=-1.18$.

ones in Figs. 1(b) and 1(c) and much thinner than the sech profile, but is shown later, by both the Evans function method and by full numerical integration of Eq. (1), to be unstable. The asymmetry, the secondary hump, and also the numerical difficulties occurring for parameter values in that region arise from the fact that, in the z plane, the right tail approaches the negative semiaxis. There $\mathrm{Ai}_{-1}(z)$ is more slowly decreasing and in some directions exhibits a small hump. Moreover, there $\mathrm{Ai}_1(z)$ is slowly growing and may be wrongly contributing to the right tail behavior produced by the first shooting strategy.

The existence pattern of solutions corresponding to B_l comprises two distinct regions: One region for β smaller than 0.11, which is limited from above by a descending $\Delta(\beta)$ curve, and another region for β larger than 0.15, which is also limited but from below by a descending $\Delta(\beta)$ curve. The absence of solutions occurs for (β,Δ) values such that $z(y_2)$ lies in a region of the complex plane where no Airy solution is rapidly decreasing to the left, i.e., $z(y_2)$ lies in the vicinity of the negative real axis. The solutions found in the region of smaller β are reasonably close to the sech profile and tanh chirp [see Fig. 2(a)]. However, the typical solution of the region of larger β is very asymmetric [see Fig. 2(b)]. Its shape suggests the existence of multihump solutions which have not been further investigated.

III. NORMAL MODE STABILITY

The stability eigenvalue problem for solutions $w(y)$ to Eq. (4) is obtained by introducing into the evolution equation (1) an expression composed of the equilibrium solution $w(y)$ plus a small complex perturbation $r(Z,y)$, namely

$$q(Z,T) = \exp(i\theta)[\sigma^2(1+\beta^2)]^{1/6}[w(y) + r(Z,y)].$$

This yields

$$i\Delta r_{Z'} + \frac{r_{yy}}{2(1+2i\beta)} + iBr_y + (y - i\Delta)r + w^2 r^* + 2|w|^2 r = 0, \tag{9}$$

where $Z' = \delta Z$. Then we seek solutions r in the form $r(Z',y) = u(y)e^{i\lambda Z'} + v^*(y)e^{-i\lambda^* Z'}$ and arrive at

$$\mathsf{L}\begin{pmatrix} u \\ v \end{pmatrix} = \lambda\Delta\begin{pmatrix} u \\ v \end{pmatrix}, \tag{10}$$

where L is the matrix operator

$$\begin{pmatrix} \dfrac{\partial_{yy}}{2(1+2i\beta)} + iB\partial_y + y - i\Delta + 2|w|^2 & w^2 \\ -(w^*)^2 & -\dfrac{\partial_{yy}}{2(1-2i\beta)} + iB\partial_y - y - i\Delta - 2|w|^2 \end{pmatrix}.$$

Normal mode stability is verified if the above eigenvalue problem has no eigenvalues with negative imaginary part. This condition is analyzed using the Evans function technique of Sec. IV.

The evolution equation (1) is found to have three invariances which should relate to a zero eigenvalue for Eq. (10) having multiplicity equal to 3. The invariances occur under constant change of phase, under translations in T and under the mapping $(Z,T,q) \mapsto (Z',T',q')$ with

$$Z' = Z + \nu, \quad T' = T - \sigma Z\nu - \tfrac{1}{2}\sigma\nu^2,$$

$$q'(Z',T') = q(Z,T)\exp\left[i\sigma\nu\left(\tfrac{1}{2}\sigma\nu Z + \tfrac{1}{6}\sigma\nu^2 - T\right)\right],$$

where ν is a real parameter [and for which $\zeta = T + \frac{1}{2}\sigma Z^2 + bZ + \zeta_0$ and $W(\zeta)$ are invariants]. The associated zero modes are $(w\ -w^*)^T$, $(w'\ (w^*)')^T$, and $(w_B\ w_B^*)^T$. However, if the solution w is the localized single-humped profile determined in Sec. II, the parameter b (or B) is not arbitrary but may only take one or two discrete values. Consequently, the derivative w_B is undefined and we expect to obtain results consistent with only two zero eigenfunctions (indeed the condition that $|q|$ decays as $T \to \pm\infty$ with q localized for all Z is not invariant under the mapping corresponding to the third invariance). However, if we were to consider general (possibly nonlocalized) solutions of Eq. (4) so that B may be taken arbitrarily, the zero eigenvalue would have multiplicity equal to 3.

IV. EVANS FUNCTION METHOD

The pulselike solutions to Eq. (4) are functions decaying rapidly in both directions. Thus, as $y \to \pm\infty$ the operator L in Eq. (10) may be replaced by its asymptotic form given by

$$\mathsf{L}_\infty = \begin{pmatrix} \dfrac{\partial_{yy}}{2(1+2i\beta)} + iB\partial_y + y - i\Delta & 0 \\ 0 & \dfrac{-\partial_{yy}}{2(1-2i\beta)} + iB\partial_y - y - i\Delta \end{pmatrix}.$$

After a manipulation similar to that applied to the linearized form of Eq. (4), the asymptotic eigenvalue problem is shown to be equivalent to two decoupled Airy equations. In fact, introducing the new variables

$$\mathcal{U}(z^+) = u(y)\exp[iB(1+2i\beta)y], \tag{11}$$

$$\mathcal{V}(z^-) = v(y)\exp[-iB(1-2i\beta)y], \tag{12}$$

and

$$z^{\pm}(y) = (2 \pm 4i\beta)^{1/3}\left(-y \pm i\Delta \pm \lambda\Delta - \frac{B^2}{2} \mp i\beta B^2\right), \tag{13}$$

we arrive at

$$\mathcal{U}'' - z^+\mathcal{U} = 0, \quad \mathcal{V}'' - z^-\mathcal{V} = 0.$$

This result permits us to use the recently implemented Evans function methodology [7] to investigate the eigenvalues of Eq. (10). A relevant eigenvalue of Eq. (10) is a value λ for which the system has a localized bounded solution. In turn, a localized solution to Eq. (10) exists whenever the stable manifold [spanned by the right-decaying solutions to Eq. (10)] and the unstable manifold (spanned by the left-decaying solutions) have nonempty intersection. As the asymptotic system is equivalent to a system of Airy equations, these right- and left-decaying solutions should relate to appropriate recessive Airy functions. Figure 3 shows corresponding typical locations of z^+ and z^- when y takes values in the real domain. They are lines of inclination $\pm\phi$, where the angle ϕ is the same as described in Sec. II given by $\phi = \frac{1}{3}\arg(2+4i\beta)$. As the imaginary part of λ is changed, the two lines move to parallel positions. Changing the real part of λ only moves $z^{\pm}$ along the respective line. The portions of these lines $[z^{\pm}(y_2), z^{\pm}(y_1)]$ corresponding to the numerical integration range we designate as *profile domains*. They move along the same line if $\mathrm{Re}(\lambda)$ is changed and move to a parallel location if, otherwise, $\mathrm{Im}(\lambda)$ is changed. Note that the intercepts of the $z^{\pm}$ lines with the real axis coincide, but depend upon the imaginary part of λ and do not necessarily occur on the negative semiaxis as in the example shown in Fig. 3. As $y \to -\infty$, z^- and z^+ lie in S_0. As $y \to +\infty$, z^- lies in S_1 and z^+ in S_{-1}. The respective recessive Airy functions are $\mathrm{Ai}_0(z^{\pm})$, $\mathrm{Ai}_1(z^-)$, and $\mathrm{Ai}_{-1}(z^+)$.

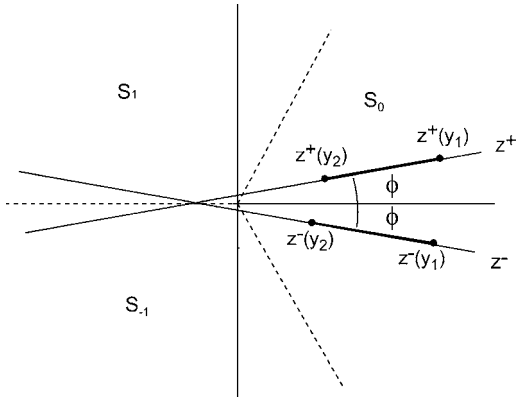

FIG. 3. $z^{\pm}$ lines and profile domains $[z^{\pm}(y_2), z^{\pm}(y_1)]$ for fixed λ.

In order to define the appropriate Evans function, we rewrite system (10) as a first-order system. For this we introduce the vector variable $Y = (u\ u_y\ v\ v_y)^T$ and arrive at

$$\frac{dY}{dy} = A(y,\lambda)Y, \tag{14}$$

where $A(y,\lambda)$ is given by

$$\begin{pmatrix} 0 & 1 & 0 & 0 \\ \mu^+[-y+\Delta(i+\lambda)-2|w|^2] & -iB\mu^+ & -\mu^+w^2 & 0 \\ 0 & 0 & 0 & 1 \\ -\mu^-(w^*)^2 & 0 & \mu^-[-y-\Delta(i+\lambda)-2|w|^2] & iB\mu^- \end{pmatrix},$$

with $\mu^{\pm} = (2 \pm 4i\beta)$. As $y \to -\infty$, there are two basis solutions to Eq. (14) which decay. Their asymptotic behavior relates to $\mathrm{Ai}_0(z)$ in the following way:

$$Y_1^-(y,\lambda) \sim Y_1^{\infty} = e^{-iB\mu^+ y/2}(\mathrm{Ai}_0(z^+) \quad -(\mu^+)^{1/3}\mathrm{Ai}_0'(z^+) - iB\mu^+\mathrm{Ai}_0(z^+) \quad 0 \quad 0)^{\mathsf{T}},$$

$$Y_2^-(y,\lambda) \sim Y_2^{\infty} = e^{iB\mu^- y/2}(0 \quad 0 \quad \mathrm{Ai}_0(z^-) \quad -(\mu^-)^{1/3}\mathrm{Ai}_0'(z^-) + iB\mu^-\mathrm{Ai}_0(z^-))^{\mathsf{T}}.$$

As $y \to +\infty$, there are also two basis solutions to Eq. (14) which decay, but in this case the asymptotic behavior relates to $\mathrm{Ai}_1(z^-)$ and $\mathrm{Ai}_{-1}(z^+)$, namely

$$Y_3^+(y,\lambda) \sim Y_3^{\infty} = e^{-iB\mu^+ y/2}(\mathrm{Ai}_{-1}(z^+) \quad -(\mu^+)^{1/3}\mathrm{Ai}_{-1}'(z^+) - iB\mu^+\mathrm{Ai}_{-1}(z^+) \quad 0 \quad 0)^{\mathsf{T}},$$

$$Y_4^+(y,\lambda) \sim Y_4^{\infty} = e^{iB\mu^- y/2}(0 \quad 0 \quad \mathrm{Ai}_1(z^-) \quad -(\mu^-)^{1/3}\mathrm{Ai}_1'(z^-) + iB\mu^-\mathrm{Ai}_1(z^-))^{\mathsf{T}}.$$

Following [7], we define an Evans function to be the Wronskian of these four vector solutions evaluated at the peak position y_p,

$$D_{\mathrm{ai}}(\lambda) = \begin{vmatrix} Y_{11}^{-}(y_p,\lambda) & Y_{21}^{-}(y_p,\lambda) & Y_{31}^{+}(y_p,\lambda) & Y_{41}^{+}(y_p,\lambda) \\ Y_{12}^{-}(y_p,\lambda) & Y_{22}^{-}(y_p,\lambda) & Y_{32}^{+}(y_p,\lambda) & Y_{42}^{+}(y_p,\lambda) \\ Y_{13}^{-}(y_p,\lambda) & Y_{23}^{-}(y_p,\lambda) & Y_{33}^{+}(y_p,\lambda) & Y_{43}^{+}(y_p,\lambda) \\ Y_{14}^{-}(y_p,\lambda) & Y_{24}^{-}(y_p,\lambda) & Y_{34}^{+}(y_p,\lambda) & Y_{44}^{+}(y_p,\lambda) \end{vmatrix}, \tag{15}$$

where $Y_{ij}^{\pm}$ $(i,j=1,\ldots,4)$ is the j component of $Y_i^{\pm}$. $D_{\mathrm{ai}}(\lambda)$ is zero if and only if the above basis solutions are linearly dependent, which happens whenever λ is an eigenvalue. $z^{\pm}$ are analytic functions of λ; the Airy functions are analytic everywhere in $\mathbb{C}$ so that Y_i^{∞} $(i=1,\ldots,4)$ are analytic functions of λ. Assuming that Y_1^{-}, Y_2^{-}, Y_3^{+}, and Y_4^{+} depend analytically on their initial data Y_i^{∞}, we conclude that $D_{\mathrm{ai}}(\lambda)$ is analytic in the eigenvalue parameter λ. The analyticity permits the use of the argument principle in searching for eigenvalues and so reduces the required work.

For each value of λ, the evaluation of $D_{\mathrm{ai}}(\lambda)$ requires the numerical computation of the four functions Y_1^{-}, Y_2^{-}, Y_3^{+}, and Y_4^{+} at $y=y_p$. Y_1^{-} and Y_2^{-} are computed separately using forward integration of system (14) from $y=y_1$ and using initial conditions taken from their asymptotic form as $y\to-\infty$, i.e., $Y_1^{\infty}(y_1,\lambda)$ and $Y_2^{\infty}(y_1,\lambda)$, respectively. These integrations finish at $y=y_p$, where $Y_1^{-}(y_p,\lambda)$ and $Y_2^{-}(y_p,\lambda)$ are recovered. Similarly, Y_3^{+} and Y_4^{+} are computed separately using backward integration of system (14) from $y=y_2$, with initial conditions $Y_3^{\infty}(y_2,\lambda)$ and $Y_4^{\infty}(y_2,\lambda)$, until $y=y_p$, where $Y_3^{+}(y_p,\lambda)$ and $Y_4^{+}(y_p,\lambda)$ are recovered. Since system (14) involves the solution w, Eq. (4) is integrated simultaneously with initial conditions as found in the shooting method described in Sec. II.

The search for eigenvalues of Eq. (14) is equivalent to the search for zeros of $D_{\mathrm{ai}}(\lambda)$. $D_{\mathrm{ai}}(\lambda)$ was evaluated as λ moves on closed paths or as λ moves along lines where eigenvalues are suspected to exist. In the former situation, as λ moves along the path, both $D_{\mathrm{ai}}(\lambda)$ and a continuous function for $\arg[D_{\mathrm{ai}}(\lambda)]$ were evaluated. Then, by the argument principle, the absolute value of the difference between the initial and final values of $\arg[D_{\mathrm{ai}}(\lambda)]$, when divided by 2π, gives the number of zeros inside the closed path. In the latter situation, the eigenvalues are located where $D_{\mathrm{ai}}=0$.

Evaluation of the Evans function as λ moves around a circle of small radius centered on $\lambda=0$ shows a change in its argument by 4π. This result asserts multiplicity equal to 2 for the zero eigenvalue, in agreement with observation in Sec. III. As anticipated by previous stability analysis, the general spectral properties of Eq. (14) are significantly different for B_s solutions and B_l solutions.

Solutions corresponding to B_s

According to the Evans function results, we can distinguish a parameter region, as shown in Fig. 4, where the solutions $w(y)$ are stable. All the B_s solutions corresponding to (β,Δ) outside this region are unstable. The region of stability has as lower boundary an existence curve (computed here for $\Delta>\frac{3}{4}\beta^{1/3}$) and as upper boundary another curve $\Delta=\Delta_{\mathrm{lim}}(\beta)$. The two curves meet around $\beta=0.88$, so closing the region. The transition occurring at $\Delta=\Delta_{\mathrm{lim}}(\beta)$ is due to a Hopf bifurcation, i.e., a pair of stable complex eigenvalues crosses the real axis and emerges in the lower half-plane as unstable eigenvalues. A further increase in Δ from the threshold value $\Delta_{\mathrm{lim}}(\beta)$ results in increasing the number of unstable eigenvalues. Moreover, the eigenvalues enter deeper into the lower half-plane, which implies larger exponential growth of the corresponding unstable modes.

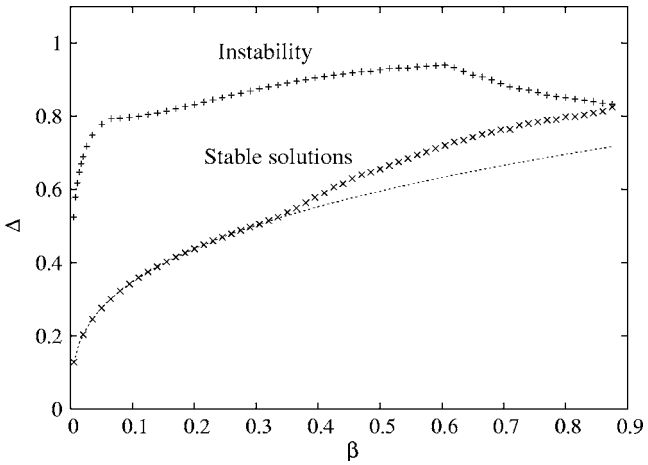

FIG. 4. Boundaries of existence and stability in the (β,Δ) plane for B_s solutions. The lower curve $(\times)$ is the existence limit and the upper curve $\Delta=\Delta_{\mathrm{lim}}(\beta)$ (denoted $+$) is the stability limit obtained by the Evans function method. The dotted curve represents $\Delta=\frac{3}{4}\beta^{1/3}$.

The procedure to search for unstable eigenvalues has used the argument principle in a quarter circle that encloses all the third or the fourth quadrants. Note that the symmetry of the eigenvalue problem guarantees that all eigenvalues occur in pairs such as $(\lambda,-\lambda^{*})$. The radius of this quarter circle was chosen as large as numerically feasible (ranging from 50 to 100) and the neighborhood of the origin was excluded to avoid the zero of $D_{\mathrm{ai}}(\lambda)$ at $\lambda=0$.

From among the stable eigenvalues, we distinguish the pure positive imaginary eigenvalue of lowest absolute value. For $\beta=0.08$ and $\Delta=0.33$, this eigenvalue assumes the value $\lambda=0.815i$ which indicates strong stability, despite the proximity to the curve $\Delta=\frac{3}{4}\beta^{1/3}$, which is the Kodama and Wabnitz prediction for the existence boundary (the corresponding eigenfunction is shown in Fig. 5). The evaluation of $D_{\mathrm{ai}}(\lambda)$ as λ moves along the positive imaginary axis revealed that, for β values up to approximately 0.6, this eigenvalue moves down to the origin as Δ decreases towards the existence boundary [curve $(\times)$ in Fig. 4]. For β small $(\beta<0.05)$, this eigenvalue eventually merges with the repeated zero eigenvalue, emerging as an unstable eigenvalue of the B_l family as explained below.

Whenever an eigenvalue, denoted by λ^{*}, is found, its eigenfunction $Y=(u\ u_y\ v\ v_y)^T$ may also be computed. For $\lambda=\lambda^{*}$, Y_1^{-}, Y_2^{-}, Y_3^{+}, and Y_4^{+} are linearly dependent, namely

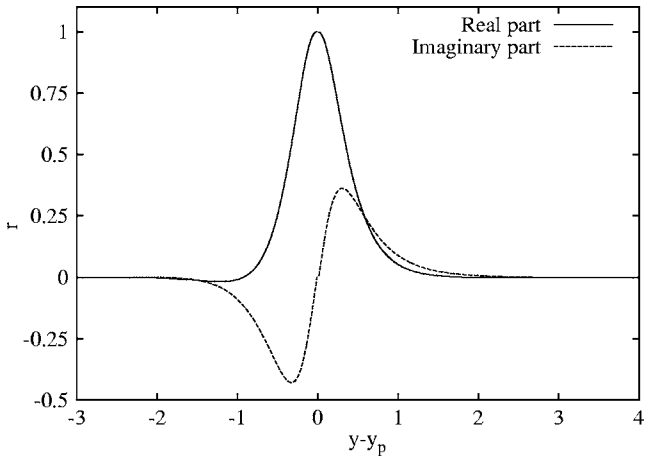

FIG. 5. Perturbation $r(0,y)$ built from the eigenfunction $(u\ v)^{\mathsf{T}}$ corresponding to $\lambda=0.815i$ for the B_s solution with $\beta=0.08$ and $\Delta=0.33$.

$$a_1 Y_1^- + a_2 Y_2^- = a_3, Y_3^+ + a_4 Y_4^+.$$

The vector $(a_1\ a_2\ -a_3\ -a)^T$ can be obtained by singular value decomposition of $D_{\text{ai}}(\lambda^*)$ and then used to construct Y from the above-computed functions.

Apart from the eigenfunction associated with $\lambda=0$, which coincides with $w(y)$, we generally found two more localized eigenfunctions similar to those in Fig. 5, belonging to the two lowest pure imaginary (positive imaginary) eigenvalues. Another type of eigenfunction is not localized within the profile domain and arises when the eigenvalues belong to the cluster of complex eigenvalues responsible for the loss of stability at the upper curve of Fig. 4. One example of this type is shown in Fig. 6. The fact that these eigenfunctions are not localized within the profile domain causes the modes to be radiationlike. Nevertheless, they should eventually decay to the left as they behave like the recessive Airy function of the corresponding sector.

The upper limit of stability determined using the Evans function method should correspond to the limit found experimentally and numerically in 1994 by Mamyshev and Mollenauer [2]. They described this as an upper energy limit above which nonsolitonic components are not completely removed by the sliding filtering. The stability boundary found here is an upper limit for Δ. For fixed β, as Δ increases, both the peak amplitude and energy increase, which confirms the correspondence between our boundary shown in Fig. 4 and the Mamyshev limit. Since 1994, the same stability limit has been analytically estimated using two different perturbation techniques [4,5]. Both works attributed the loss of stability to the growth of dispersive radiation. Likewise, the Evans function method, applied here, predicts the loss of stability whenever a radiationlike mode crosses the real axis and becomes unstable.

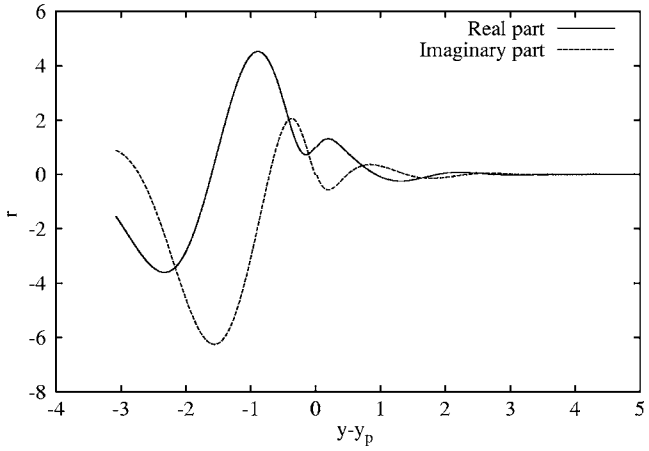

FIG. 6. Perturbation $r(0,y)$ built from the eigenfunction $(u\ v)^{\mathsf{T}}$ corresponding to $\lambda=\pm 6.24-\epsilon i$ for the B_s solution with $\beta=0.5$ and $\Delta=0.93$.

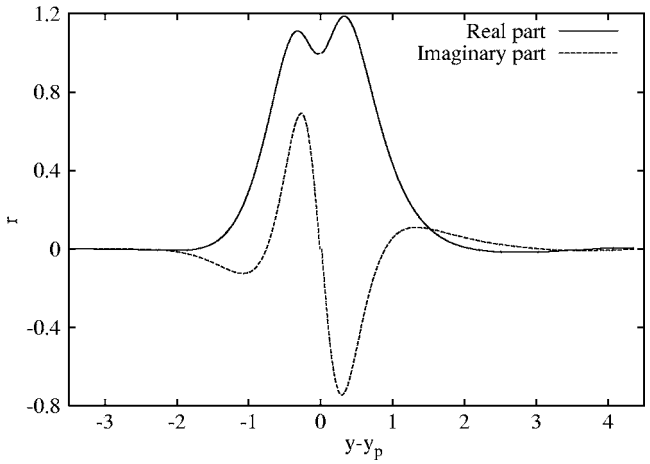

FIG. 7. Perturbation $r(0,y)$ built from the eigenfunction $(u\ v)^{\mathsf{T}}$ corresponding to $\lambda=-0.717i$ for the B_l solution with $\beta=0.08$ and $\Delta=0.33$.

Solutions corresponding to B_l

As pointed out in Sec. II, there are two types of B_l solutions, one more symmetrical occurring for smaller values of β and another significantly asymmetrical existing for larger values of β. The Evans function method can be applied to study the stability of the former type, however, in general, this method cannot be applied to the asymmetric type since the backward integration of Eq. (4) from the corresponding y_2 is not numerically feasible. Whenever applied, the Evans method revealed one pure negative imaginary eigenvalue for all the solutions of the first kind, which confirms the unstable classification given by the perturbation technique [3] to B_l solutions. This unstable eigenvalue λ_u was found to be confined to a portion of the negative imaginary axis, i.e., $\lambda_u=-\rho i$ with $0\leqslant\rho\lesssim 1.47$. The eigenvalue takes the limit value $\lambda_u=0$ at the boundary $\Delta\approx\frac{3}{4}\beta^{1/3}$, and as Δ is increased and β fixed, it moves toward $-1.47i$. Then, if Δ is further increased, the eigenvalue reverses its direction. Nevertheless, the upper Δ limit is always reached before λ_u comes close to zero again. Figure 7 shows one example of those unstable modes.

V. DIRECT NUMERICAL INTEGRATION

To confirm the regime of accelerating pulses and the stability results, the numerical simulation of the evolution equa-

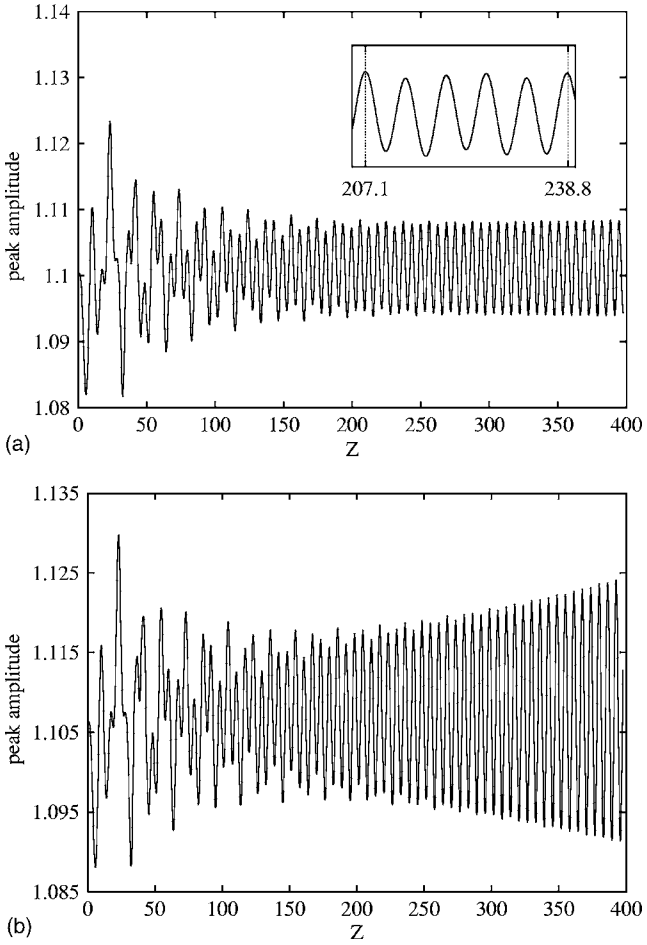

FIG. 8. Peak amplitude evolution of an initial pulse corresponding to $\beta=0.5$, $\sigma=0.05$, $B=B_s$, and (a) $\Delta=0.93$, (b) $\Delta=0.95$. Inset in (a) shows the period of oscillation. Note that $\Delta_{\mathrm{lim}}(0.5)\approx 0.927$.

tion (1) was performed using the self-similar pulses as initial conditions. The numerical integration of Eq. (1) confirmed the location of the upper stability boundary $\Delta=\Delta_{\mathrm{lim}}(\beta)$. For $\Delta\approx\Delta_{\mathrm{lim}}(\beta)$, the peak amplitude undergoes oscillations whose period is in agreement with the eigenvalue that crosses the real axis at this boundary. For example, the period of oscillation shown in the inset of Fig. 8(a) is $T\simeq 6.34$ and the crossing eigenvalue for these values of β and Δ is $\lambda=\pm 6.24$, confirming the predicted relation $T=2\pi/\lambda\delta$ (note that $\sigma=0.05$ and consequently $\delta=0.159$). These oscillations are decaying if Δ is slightly below the boundary and growing otherwise [Fig. 8(b)]. Whenever the propagation is stable, the trajectory is in good agreement with the predicted parabolic path $T=T_0-bZ-\sigma Z^2/2$.

Direct numerical integration revealed severe instability of the asymmetrical B_l solutions shown by the example in Fig. 2(b) and confirmed the instability of the symmetrical B_l solutions [example in Fig. 2(a)] as predicted by the Evans method. Figure 9 shows the peak amplitude evolution for two symmetrical B_l solutions where the typical decaying behavior is present. Note that the solution corresponding to larger Δ has a more rapid decay. The estimated growth rate of the unstable modes is $\delta\lambda$, which gives 0.032 for the $\Delta=0.33$ solution and 0.073 for the $\Delta=0.39$ solution.

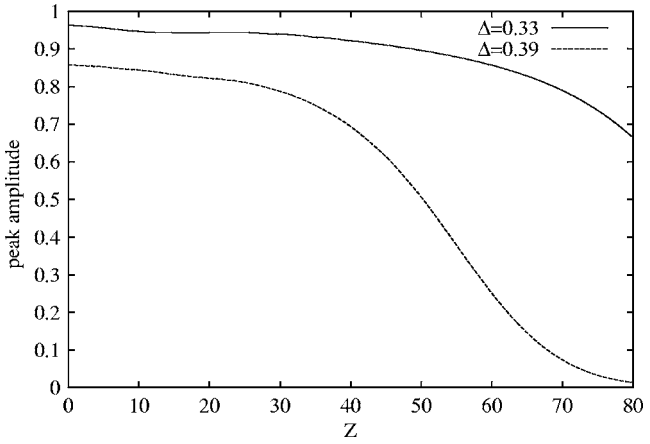

FIG. 9. Evolution of peak amplitude for two B_l solutions with $\beta=0.08$, $\Delta=0.33, 0.39$, and $\sigma=0.05$.

VI. CONCLUSION

We found equilibrium solutions for the sliding filtering model described by Eq. (1) for a wide range of filter strength values (β ranging up to 2.0) using an accelerating similarity variable reduction. In general, for each choice of parameters, there are two equilibrium solutions which differ in velocity and peak amplitude. The stability of such solutions was then studied using the Evans method, which has been recently adapted to accelerating solutions. The low peak amplitude solutions which correspond to larger velocity modulus (B_l solutions) were found unstable. For small β, the stability analysis was performed by the Evans method but for larger β the instability was only recognized by full numerical integration of Eq. (1) using the equilibrium solutions as initial condition. Using the Evans method, we were also able to distinguish a parameter region where the high peak amplitude solutions (B_s solutions) are stable. For fixed filter strength β and sliding rate σ, the loss of stability occurs for an upper limit of excess gain δ and is due to a Hopf bifurcation. The stability threshold and the type of eigenvalues/eigenfunctions responsible for the stability transition is in agreement with previously published results. The value of those transition eigenvalues can actually be found by the Evans method, thus we can predict the frequency of the peak amplitude oscillations exhibited by the pulse along the propagation distance. Below the Δ threshold, i.e., within the stability region, those amplitude oscillations are decaying, but otherwise they grow. Full numerical integration of the evolution equation was also performed which has confirmed those stability results. Note that, for practical purposes, for each σ and β, the stability limits in Δ (as shown in Fig. 4 for generic σ) may be readily converted to lower and upper limits in pulse power. Moreover, our technique for finding the equilibrium solutions predicts the actual width and the existence of possible secondary humps which can be valuable in order to prevent interaction between adjacent pulses.

ACKNOWLEDGMENT

M.F. acknowledges the support of Fundação para a Ciência e a Tecnologia, Portugal.

[1] L. F. Mollenauer, J. P. Gordon, and S. G. Evangelides, Opt. Lett. **17**, 1575 (1992).
[2] P. V. Mamyshev and L. F. Mollenauer, Opt. Lett. **19**, 2083 (1994).
[3] Y. Kodama and S. Wabnitz, Opt. Lett. **19**, 162 (1994).
[4] S. Burtsev and D. J. Kaup, J. Opt. Soc. Am. B **14**, 627 (1997).
[5] J. J. Beech-Brandt and N. F. Smyth, Phys. Rev. E **63**, 056604 (2001).
[6] D. F. Parker, C. Radha, and M. Facão, Phys. Rev. E **65**, 066615 (2002).
[7] M. Facão and D. F. Parker, Phys. Rev. E **68**, 016610 (2003).
[8] F. W. J. Olver, *Asymptotics and Special Functions* (Academic, New York, 1973).